Electron Pinball and Commensurate Orbits in a Periodic Array of Scatterers

D. Weiss,[1],[2] M. L. Roukes,[1] A. Menschig,[3] P. Grambow,[2] K. von Klitzing,[2] and G. Weimann[4]

[1]Bellcore, Red Bank, New Jersey 07701
[2]Max Planck Institut für Festkörperforschung, D-7000 Stuttgart 80, Germany
[3]IV Physikalisches Institut der Universität Stuttgart, D-7000 Stuttgart 80, Germany
[4]Walter-Schottky Institut der Technische Universität München, D-8046 Garching, Germany
(Received 15 November 1990)

We have introduced an artificial array of scatterers into a *macroscopic* two-dimensional conductor nearly devoid of intrinsic defects. This generates pronounced structure in the magnetoresistance, anomalous low-field Hall plateaus, and a quenching of the Hall effect about $B=0$. Our calculations show that the predominant features in the data arise from commensurate classical orbits impaled upon small groups of the imposed scatterers.

PACS numbers: 73.50.Dn, 72.10.Fk

Generally, impurity scattering is considered to be a stochastic process. Electrons collide with defects located *randomly* throughout a conductor. In this Letter, electron transport is studied in an unusual situation: We lithographically impose a *periodic* lattice of strong scatterers upon a relatively defect-free two-dimensional electron gas (2DEG). We accomplish this by etching an array of microscopic holes into a high-mobility 2DEG conductor. Introduction of this strong spatially modulated potential leads to dramatic commensurability effects at low temperatures in an applied magnetic field. Pronounced structure is manifested in the magnetoresistance at low B. We find that the predominant features can be explained classically, but many interesting, and anomalous, properties of this system appear beyond the scope of simple electron-orbit analysis.

Recently, it has been observed that magnetoresistance oscillations periodic in $1/B$ emerge at low magnetic fields when a high-mobility 2DEG is subjected to a *weak* periodic 1D potential.[1] This phenomenon is attributed to the formation of Landau bands due to the soft lateral superlattice potential.[2–4] Preliminary work in 2DEG systems involving *strong* periodic potentials indicates that entirely different behavior is to be expected.[5–9] We shall explore this in detail below.

We fabricate samples from high-mobility GaAs-AlGaAs heterojunctions. At 4 K, before patterning, these have carrier densities between $n_s \sim 2.2\times10^{11}$ and 3.0×10^{11} cm^{-2} and mobilities from $\mu_0 \sim 0.56\times10^6$ to 1.2×10^6 cm^2/Vs. The corresponding transport mean free path, $l_0 = m^* v_F \mu_0/e$, ranges between 4.4 and 9.6 μm. Here, v_F is the Fermi velocity and m^* the effective mass. A periodic (square) lattice of scatterers is introduced by etching an array of holes (lithographic diameters d_{lith} with period a) into a 100-μm-wide Hall bar patterned from the 2DEG by conventional techniques (Fig. 1, insets). The periodic array is defined by electron-beam lithography and transferred into the 2DEG by dry etching.[10] Note that although $l_0 \gg a$, the Hall bar itself is *macroscopic;* its dimensions are large compared to l_0. The device geometry allows comparison of the resistivity (ρ_{xx}) and the Hall resistance (ρ_{xy}) from both patterned and unpatterned segments of the same sample.

The imposed array of "antidots" dramatically affects transport at low B (Fig. 1). The enhanced $\rho_{xx}(B=0)$ reflects reduced mobility at low B ($\mu'=4\times10^4$ cm^2/Vs), i.e., a mean free path ($l' \sim 0.34$ μm) comparable to a, the spacing between the imposed scatterers. New peaks at low B are accompanied by (nonquantized) steps in ρ_{xy}, and the Hall effect is quenched about $B=0$. Arrows in Fig. 1, which closely correlate with these features, mark field positions where the normalized cyclotron radius, $\hat{r}_c = r_c/a$, equals $\frac{1}{2}$ and $\frac{3}{2}$. When $\hat{r}_c < \frac{1}{2}$, ρ_{xx} drops
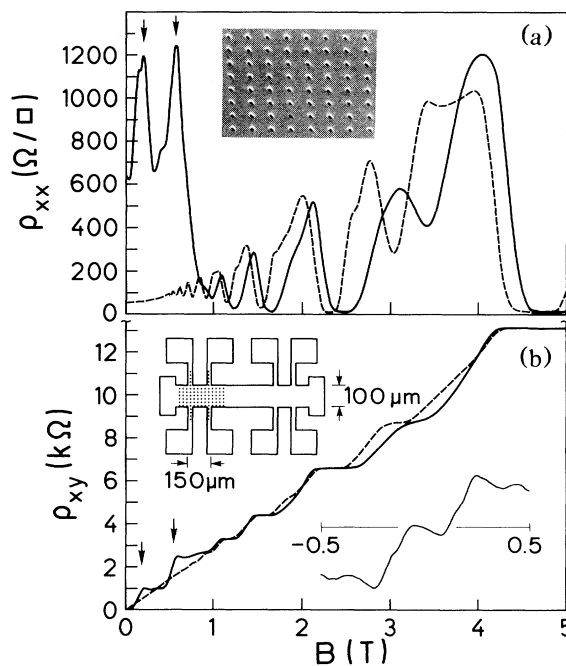

FIG. 1. (a) Magnetoresistance and (b) Hall resistance measured in patterned (solid line) and unpatterned (dashed line) sample segments at 1.5 K after brief illumination. In the patterned segment, n_s (determined from Shubnikov–de Haas oscillations) is ~8% higher ($n_s = 2.4\times10^{11}$ cm^{-2}). Top insets of (a) and (b): Electron micrograph of the "antidot" array (300 nm period) and a sketch of the sample geometry. Bottom inset of (b): Magnification of the quench in ρ_{xy} about $B=0$.

quickly, quantum oscillations commence, and ρ_{xy} begins to display accurately quantized plateaus. In this (quantum Hall) regime traces from patterned and unpatterned segments become essentially identical. This suggests that the intrinsic mobility is preserved after patterning.

Magnetoresistance curves from three samples (Table I) are compared in Fig. 2. In traces with smaller zero-field resistance a progressively greater number of peaks in ρ_{xx}, and steps in ρ_{xy}, become resolved. Their emergence is controlled by two parameters: the (normalized) antidot cross section, $\hat{d} = d/a$, and n_s.[11] Here, the *effective* cross section of the extrinsic scatterers, $d = d_{\text{lith}} + 2 \times l_{\text{depl}}$, involves the depletion length[12] l_{depl}, itself dependent upon n_s. Brief illumination of the samples at low temperature enhances n_s via persistent photoconductivity and reduces l_{depl}. Figure 2 and Table I suggest richer low field structure emerges for small values of $\hat{d}$. Sample 3^* ($\hat{d} \sim \frac{1}{3}$) exhibits the largest sequence of new ρ_{xx} peaks and ρ_{xy} plateaus. At each peak, $\hat{r}_c$ can be associated with a commensurate orbit encircling a specific number, n, of "antidots" (Fig. 2, inset). This observation motivates the explanation we present below.

The striking features described above occur at low B, in a regime where electron orbits encompass a large number of flux quanta. In this field regime, Landau quantization is suppressed in unpatterned samples when $T \geq 1.5$ K [Fig. 1(a)], while the microstructure-induced anomalies continue to be manifested up to temperatures $T \sim 50$ K. This suggests that a classical description involving commensurate orbits, but *not* involving orbit quantization, might account for the predominant structure. At low B, when thermal broadening of the Landau levels is significant ($k_B T > \hbar \omega_c$), magnetotransport is described by the Drude model. In an ideal *unpatterned* 2DEG, with B applied normally, carriers perform cyclotron orbits with radius $r_c = v_F/\omega_c$ and angular frequency $\omega_c = eB/m^*$. For $\omega_c \tau < 2\pi$, scattering terminates the motion before a full orbit is completed. Here τ is the intrinsic momentum relaxation time, reflecting interactions between electrons and, e.g., intrinsic impurities, phonons, etc. For $\omega_c \tau \gg 2\pi$, despite the circular trajectories, bulk current flows in the conductor since orbits drift with velocity $v_d = E_H/B$ in the Hall field E_H established.

Within this classical picture the magnetoresistance is B independent, $\rho_{xx} = m^*/n_s e^2 \tau \equiv \rho_0$, and the Hall resistance rises linearly, $\rho_{xy} = B/n_s e \equiv R_0 B$ (R_0 is the Hall coefficient).

To understand magnetotransport at low B in the *patterned* samples we envision transport as involving three distinct "pools" of carriers: *pinned* orbits, *drifting* orbits, and *scattered* orbits. In a patterned sample each contingent contributes to the total resistivity, which is obtained from the inverted sum of the individual conductivity tensors.

The resistivities (ρ_p, ρ_d, ρ_s) and Hall coefficients (R_p, R_d, R_s) for the pinned, drifting, and scattered carriers each depend upon (normalized) magnetic field, $1/\hat{r}_c$. We evaluate these making the simplifying assumption that the imposed potential rises quickly near each antidot, while remaining essentially flat in between. In this approximation, valid when $l_{\text{depl}} \ll a - d_{\text{lith}}$ (and especially relevant for the case of sample 3^*), electrons interact with the fabrication-imposed electrostatic potential only in the immediate locale of each antidot—elsewhere carriers move freely in the applied fields.

Pinned orbits, within this simple picture, remain localized about their orbit centers and cannot contribute to transport; hence $\rho_p = \infty$ and $R_p = 0$. Nonetheless, they play a central role in the story since *they remove a fraction $f_p(\hat{r}_c)$ of carriers from the transport process.*[13] As in a pinball game, the *scattered* orbits constitute the col-

Sample	$10^{-11} n_s$ (cm^{-2})	a (nm)	d_{lith} (nm)	l' (nm)	$\hat{d}_{\text{est}}$ [a]
1	1.4	300	60	100	0.71 ± 0.06
1^*	2.4	300	60	340	0.48 ± 0.09
2	Depleted	200	70	$\cdots$	$\cdots$
2^*	2.0	200	70	120	0.47 ± 0.03
3	2.8	300	40	600	0.39 ± 0.08
3^*	3.7	300	40	720	0.33 ± 0.08

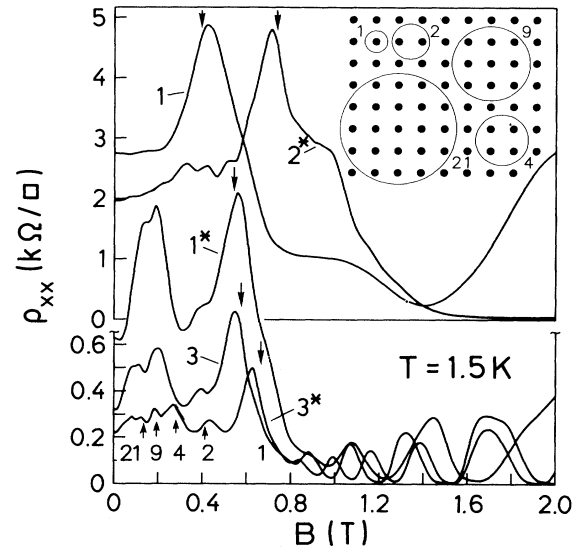[a]Estimate from decay of ρ_{xx} at high B: $f_s \to 0$ when $\hat{r}_c \leq (1 - \hat{d})/2$.

FIG. 2. Low-B anomalies from samples of three different heterojunctions (see Table I). Arrows mark $\hat{r}_c = \frac{1}{2}$ for each trace. Illumination of sample 1 ($1 \to 1^*$) increases n_s by only a small factor (~ 1.7), whereas $\rho_{xx}(B=0)$ drops almost by a factor of 5. This indicates that l_{depl} and, consequently, $\hat{d}$ are reduced after illumination. For smaller $\hat{d}$ more structure in ρ_{xx} becomes resolved. Peaks in trace 3^* can be ascribed to commensurate orbits with $n = 1$, 2, 4, 9, and 21, as sketched in the inset (for $\hat{d} = \frac{1}{3}$ and average $\hat{r}_c = 0.5$, 0.8, 1.14, 1.7, and 2.53, respectively).
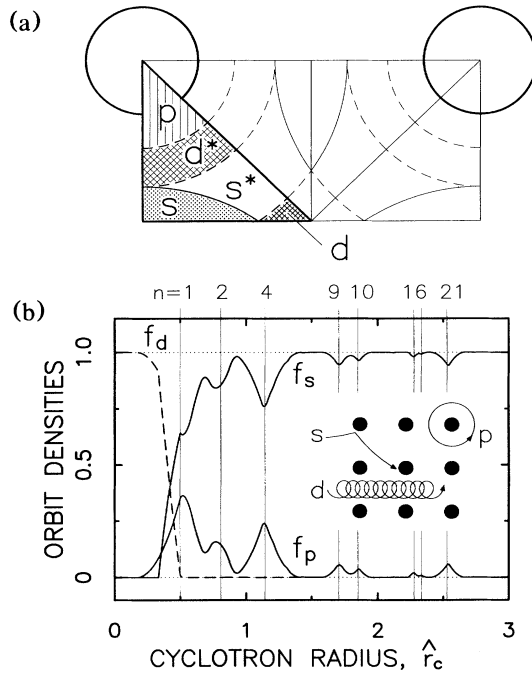
(a)

(b)

FIG. 3. One-eighth of the real-space zone diagram constructed for one specific value of $\hat{r}_c$ (0.44) for a square lattice of cross section $\hat{d} = \frac{1}{3}$. Pinned, scattering, and drifting orbits have centers within regions marked p, s, and d, respectively. The fraction of area within each zone directly determines that contingent's density. The zone d^* comprises skipping orbits, assumed here to be a subset of the drifting contingent (see Ref. 14). Orbit centers within s^* precess about an antidot, and then scatter in the zone s. (b) Orbit densities vs $\hat{r}_c$. Fine lines demark average $\hat{r}_c$ values of orbits impaled upon $n = 1$, 2, 4, 9, 10, 16, and 21 antidots.

lection of paths (arcs) leading between pairs of antidots. At low B, where $\hat{r}_c$ is large, it is primarily these uncompleted "orbits" which carry current through the conductor. This fraction of carriers $f_s(\hat{r}_c)$ scatters with an *effective* relaxation time $\tau' = (\tau^{-1} + \tau_{ex}^{-1})^{-1}$. Here, τ^{-1} and τ_{ex}^{-1} are the intrinsic and extrinsic rates. Transport coefficients for scattered carriers are thus $\rho_s = \rho_0 \tau / f_s \tau'$ and $R_s = R_0 / f_s$. At high B, however, it is *drifting* orbits, involving the fraction $f_d(\hat{r}_c)$ of carriers, which dominate transport. These behave as if in an unpatterned sample; for them $\rho_d = \rho_0 / f_d$ and $R_d = R_0 / f_d$.[14]

These extensions of the Drude picture to describe a *periodic* lattice of scatterers yield (normalized) expressions for the total resistivity,

$$\frac{\rho}{\rho_0} = \frac{\tau(\tau' f_s + \tau f_d) + \tau'(\tau f_s + \tau' f_d)\omega_c^2 \tau^2}{(\tau' f_s + \tau f_d)^2 + \tau'^2(1 - f_p)^2 \omega_c^2 \tau^2}, \quad (1)$$

and Hall coefficient,

$$\frac{R}{R_0} = \frac{\tau'^2 f_s + \tau^2 f_d + \tau'^2(1 - f_p)\omega_c^2 \tau^2}{(\tau' f_s + \tau f_d)^2 + \tau'^2(1 - f_p)^2 \omega_c^2 \tau^2}. \quad (2)$$

These explicitly relate transport coefficients to $\hat{r}_c$-

dependent orbit densities and scattering rates. At low B [specifically, for $\hat{r}_c > (\sqrt{2} - \hat{d})/2$] drifting orbits vanish, hence $f_s = 1 - f_p$, and transport involves only the *scattered* orbits: $\rho \rightarrow \rho_s$ and $R \rightarrow R_s$.

For intermediate to high B the orbit densities can be ascertained by a simple geometric construction, specific for a given $\hat{r}_c$ [e.g., Fig. 3(a) where $\hat{r}_c = 0.44$]. This delineates zones within the real-space unit cell associated with each contingent of electrons, based on orbit-center positions. As $\hat{r}_c$ increases, this zone diagram becomes increasingly complex—a heirarchy of pinned orbits, which surround progressively greater numbers of antidots, unfolds.[15] In this regime geometric analysis becomes impractical and we resort to straightforward numerical calculation of the f's.[16] In Fig. 3(b) orbit densities calculated for $\hat{d} = \frac{1}{3}$ are seen to display pronounced commensurability effects. For larger values of $\hat{d}$ both calculations[17] and experiments (Fig. 2) show that structure for $n > 1$ becomes suppressed.

As a first approximation, we may assume that the effective mean free path of scattered electrons, $l' = v_F \tau'$, is $\hat{r}_c$ independent. This has been confirmed by calculations of l' for the case of complete memory loss after a single antidot collision; these shall be described elsewhere.[17] For sample 3* with $\hat{d} \sim \frac{1}{3}$, the intrinsic mean free path is $\hat{l} \equiv v_F \tau / a \sim l_0 / a \sim 33$, while ρ_{xx} at low B indicates $l'/a = 2.4$ (Table I). The calculations show l' is nearly constant and featureless for these same values of $\hat{l}$ and $\hat{d}$ when $\hat{r}_c$ is in the relevant range $1.2 < \hat{r}_c < 20$. In this range l'/a saturates at a value ~ 2.54, in close agreement with experiment.

We compare calculated results to experimental data in Fig. 4. Remarkable similarities are evident: $n = 1$, 2, and 4 commensurability effects are prominent in both ρ_{xx} and ρ_{xy}. In the experimental trace, surprisingly, we find clearly resolved $n = 9$ and 21 features. Our calculations predict these to be quite weak, even for smaller $\hat{d}$. We attribute their enhancement in real samples to the finite potential gradient between antidots. This should act to "guide" electrons around the antidots, permitting deviations from strictly circular trajectories (as assumed in the model) and enhancing f_p. For large $\hat{d}$ (Table I) this potential gradient becomes significant and our simple model is inapplicable. The peak at $\hat{r}_c \sim \frac{3}{2}$ in samples 1* and 3 is strongly forbidden for strictly *circular* orbits when $\hat{d} \geq \frac{1}{3}$. Despite the more complicated dynamics of such samples, our simple approach elucidates the origin of the dominant structure observed.

Well-resolved commensurability features emerge when the intrinsic mobility is maintained between the imposed scatterers and the lattice is "open" (small $\hat{d}$). In Refs. 8 and 9 it appears that these conditions (respectively) were not achieved. Recent results from a hexagonal "antidot" array,[7] previously not fully explained, can also be accounted for by our simple model.

Quenching of the Hall effect is seen in the data at low B, yet is absent from our calculated traces. Experiments
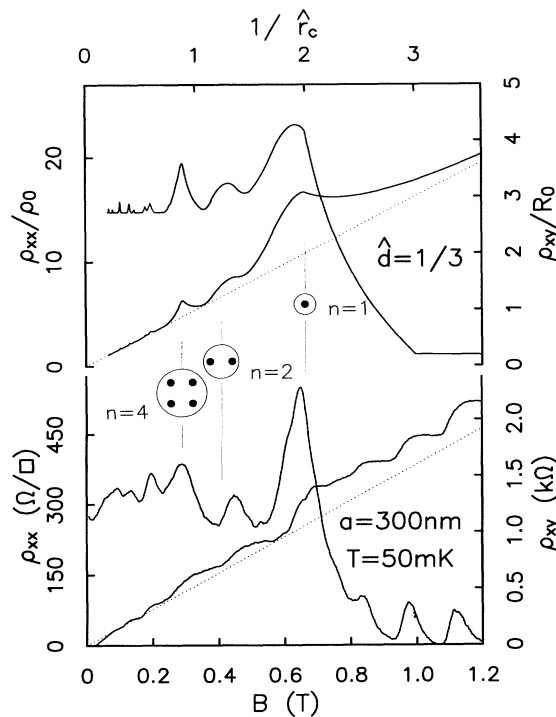
FIG. 4. Comparison between the simple model (top) and experiment (bottom). Calculated curves are obtained assuming a *constant* effective mean free path for extrinsically scattered carriers, $l'/a \sim 2.4$, and an intrinsic value $l/a \sim 33$ (values taken from experiment). Features attributed to $n = 1$, 2, and 4 pinned orbits are denoted. Very weak temperature dependence is observed experimentally for 50 mK $< T <$ 4.2 K.

in *mesoscopic* junctions,[18] and subsequent theory,[19] indicate this is a classical phenomenon requiring a component of specular reflection from the boundaries. Both demonstrate that strictly *zero*, even negative, low-B Hall coefficients can result. The extensions of the Drude model developed here implicitly involve a relaxation-time approximation for extrinsic collisions, valid when scattering from the antidots is *diffuse*. This clearly precludes accounting for phenomena, such as quenching, involving correlated multiple reflections. The agreement of our model with experiment emphasizes that low-B commensurability effects originate from a different mechanism.

Our experiments verge on the quantum regime. For example, data from sample 2* with the smallest a (Fig. 2) show three weak oscillations near 0.4 T. These features, not reproduced by our classical model, are separated by a field (~ 0.1 T) corresponding to addition of one flux quantum through the unit cell. Quantum behavior should clearly emerge with further reduction of the lattice constant. In this realm, the energy spectrum is known to be self-similar, and exotic consequences are expected in transport.[20] Manifestations of this irregular spectrum have recently been obtained from samples with weak periodic potentials.[21]

[1]D. Weiss *et al.*, Europhys. Lett. **8**, 179 (1989).

[2]R. R. Gerhardts, D. Weiss, and K. von Klitzing, Phys. Rev. Lett. **62**, 1173 (1989).

[3]R. W. Winkler, J. P. Kotthaus, and K. Ploog, Phys. Rev. Lett. **62**, 1177 (1989).

[4]E. S. Alves *et al.*, J. Phys. Condens. Matter **1**, 8252 (1989).

[5]M. L. Roukes and A. Scherer, Bull. Am. Phys. Soc. **34**, 633 (1989); A. Scherer and B. P. van der Gaag, Proc. SPIE **1284**, 149 (1990).

[6]C. G. Smith *et al.*, J. Phys. Condens. Matter **2**, 3405 (1990).

[7]H. Fang and P. J. Stiles, Phys. Rev. B **41**, 10171 (1990).

[8]K. Ensslin and P. M. Petroff, Phys. Rev. B **41**, 12307 (1990).

[9]J. P. Kotthaus, in *Granular Nanoelectronics* (Plenum, London, 1990).

[10]D. Weiss *et al.*, Appl. Phys. Lett. (to be published).

[11]At low B, ρ_{xx} is only weakly dependent upon μ_0 since long l_0 implies τ' is dominated by τ_{ex} (see text).

[12]A. Scherer and M. L. Roukes, Appl. Phys. Lett. **55**, 377 (1989); T. Demel *et al.*, *ibid.* **53**, 2176 (1988).

[13]For impaled orbits, the repulsive potential at each antidot provides a local restoring force against drift induced by electric fields. The "removal" of an electron from transport requires a long pinned orbit lifetime, $\tau_{pin} > a/v_F \sim \tau_{ex}$, obtained when μ_0 is preserved between antidots and E_H is small.

[14]At high B, a drifting electron encountering an antidot will briefly skip about its periphery. Its orbit center then precesses, stepwise, to the back side where it is ultimately freed, once again, to drift away. Here, we assume a short dwell time and equate skipping to drifting orbits.

[15]In related work, T Geisel *et al.*, Phys. Rev. Lett. **64**, 1581 (1990), describe chaotic classical dynamics.

[16]At each value of $\hat{r}_c$ we calculate f_p as the fraction of *completed* electron orbits with centers on a grid of $\sim 10^5$ sites within the real-space unit cell [M. L. Roukes (unpublished)]. For $\hat{r}_c > (\sqrt{2} - \hat{d})/2$, $f_d = 0$, and hence $f_s = 1 - f_p$.

[17]Roukes (Ref. 16).

[18]M. L. Roukes *et al.*, Phys. Rev. Lett. **59**, 3011 (1987); **64**, 1154 (1990).

[19]C. W. J. Beenakker and H. van Houten, Phys. Rev. Lett. **63**, 1857 (1989).

[20]P. G. Harper, Proc. Phys. Soc. London A **68**, 874 (1955); M. Ya. Azbel, Zh. Eksp. Teor. Fiz. **46**, 929 (1964) [Sov. Phys. JETP **19**, 634 (1964)]; D. R. Hofstadter, Phys. Rev. B **14**, 2239 (1976).

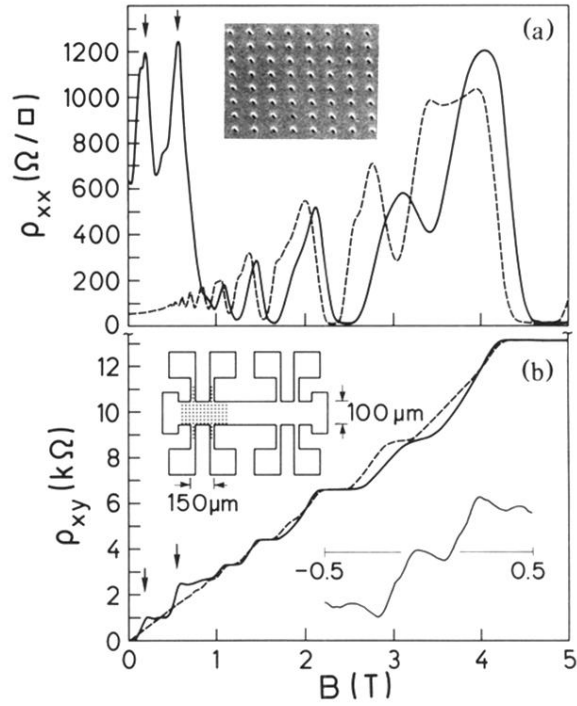[21]R. R. Gerhardts, D. Weiss, and U. Wulf, Phys. Rev. B **43**, 5192 (1991).

FIG. 1. (a) Magnetoresistance and (b) Hall resistance measured in patterned (solid line) and unpatterned (dashed line) sample segments at 1.5 K after brief illumination. In the patterned segment, n_s (determined from Shubnikov–de Haas oscillations) is ~8% higher ($n_s = 2.4 \times 10^{11}$ cm^{-2}). Top insets of (a) and (b): Electron micrograph of the "antidot" array (300 nm period) and a sketch of the sample geometry. Bottom inset of (b): Magnification of the quench in ρ_{xy} about $B = 0$.